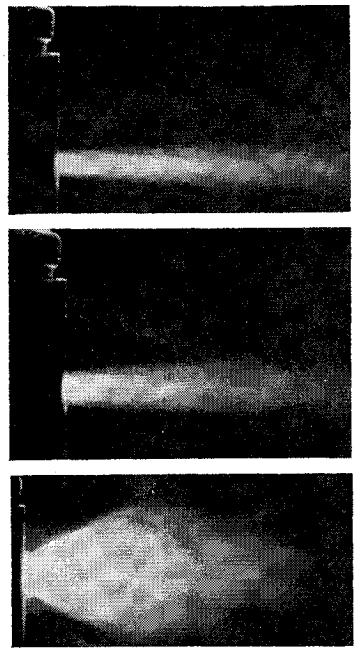

Fig. 2 Photographs of scattered light from particle plumes.

with a throat diameter of 0.260 in. and an expansion cone half-angle of 15° with an area ratio of 3.87.

The theoretical calculations show that particle trajectories depend upon the initial position of the particle, the nozzle contour (especially the subsonic convergent portion), gas stagnation pressure, and particle size and specific gravity. As the particle size decreases, the particle plume boundary for that size moves further from the plume axis; that is, the size-dependent limiting streamlines subtend a greater included angle. Thus, for a given size distribution, the outer boundary should be formed by the smaller size particles. In order to compare theory with experiment, a light scattering technique was employed. A two-dimensional sheet of visible light was passed through a cold gas-particle plume so that the plume axis lay in the plane of the light beam. Photographs of the light scattered in a direction normal to the sheet were taken to visualize the plume. The quantity of light scattered from a volume element depends upon the concentration of scatters there, so that regions of high particle concentration appear brighter in the photographic image.

Three powders with different minimum sizes were used to show the effect of particle size. Two size distributions were of glass beads, approximately 90% spheres, and one of alumina (see Fig. 1). From photographs taken with the electron microscope, the smallest alumina particle was found to be roughly 0.25 μ in radius with the most abundant size at about 0.8 μ. In contrast, the smallest glass particles for the two size distributions were about 1.0 and 5.0 μ, respectively. Photographs of the scattered light are shown in Fig. 2. In each case, the chamber pressure was 100 psig, exit pressure 200 mm Hg, tank pressure 4 mm Hg, and the particle mass flow rate to gas flow rate ratio was 0.3. The computer program was used to determine the limiting streamline radial location at the exit plane of the nozzle as a function of particle size as shown in Fig. 3. The diameter of the particle plume at the exit plane D, as obtained from the photographs, was compared with the diameter calculated for the limiting streamlines for the minimum particle size in each distribution. The good agreement between experiment and theory, shown in Table 1, is taken as a demonstration of the validity of the theory.

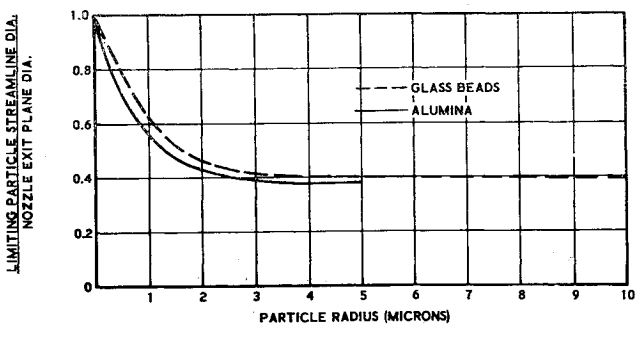

Fig. 3 Location of limiting particle streamline at the nozzle exit as a function of particle size.

Table 1 Comparison of experiment and theory for particles with radii corresponding to the lower limit of the size distribution

	Minimum particle radius, μ	$\left(\frac{D}{D_{exit}}\right)_{expt}$	$\left(\frac{D}{D_{exit}}\right)_{theo}$
Glass beads	5	0.4	0.40
Glass beads	1	0.6	0.62
Alumina	$\frac{1}{4}$	1.0	0.85

Reference

[1] Carlson, D. J., "Measurement of velocity lag of condensed phases in gas-particle nozzle flows," AIAA J. (submitted for publication).

Effect of Azimuth on the Accuracy of an Interferometer Radar

C. W. Pittman*
Aerospace Corporation, Los Angeles, Calif.

Introduction

An interferometer radar measures the position and/or velocity of a target by determining the range and/or range rate of the target from a number of tracking stations simultaneously. At least three measurements are required. A coordinate transformation to polar or rectangular coordinates is then performed by a calculation that is geometrically equivalent to finding the point of intersection of three spheres. The angle measurements from the central station (azimuth and elevation) are found to be primarily functions of the range (or range rate) differences between the stations denoted as p and q. Errors in p and q (or $\dot{p}$ and $\dot{q}$) will result in errors in A and E (or $\dot{A}$ and $\dot{E}$).

The General Electric (GE) Mod III Atlas guidance system at the Eastman Test Range (ETR) uses a doppler-measuring interferometer subsystem with three ground stations in an L configuration. In the analysis that follows, it is shown that 1) the errors in $\dot{p}$ and $\dot{q}$ behave to a considerable extent as if they originated in three independent noise sources (i.e., each of the ground stations); and 2) if this is so, then the angular rate accuracy of the subsystem is a function of the azimuth of the target relative to the baselines between the ground stations.

Figure 1 illustrates the variation in accuracy as a function of azimuth. Note that it is assumed that the raw measurement accuracy at each of the stations does not vary with azimuth. The variation is due to the changing sensitivity of the angular rates with respect to the raw measurements.

Received August 3, 1964.

* Manager, Radio Analysis Section, Electronics Division.

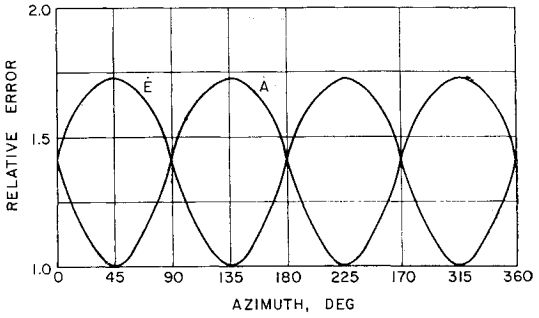

Fig. 1 Sensitivity of angular rate errors to noise on $\dot{p}$ and $\dot{q}$.

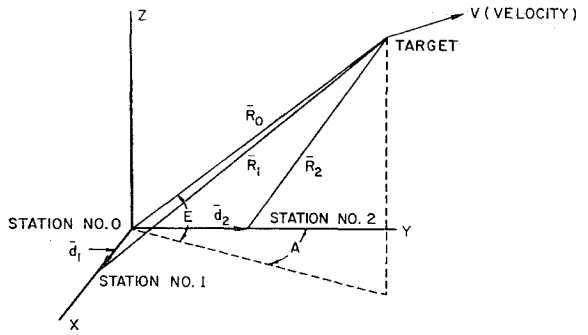

Fig. 2 Geometry of system.

Figure 2 illustrates the geometry used in the analysis. For simplicity, it is assumed that the baselines between the stations are equal in length and at right angles to each other. A rectangular coordinate frame is used with the origin at the central station and the x and y axes along the baselines. In this report, the analysis is applied to a rate-measuring system, but the results are equally valid for a position-measuring system.

Cross-Correlation between p and q

From Fig. 2, assume that the three stations are simultaneously measuring the respective range rates and that errors are included in each measurement. For simplicity, let us consider that each error is made up of two components, one of which is common to all three stations (e.g., the errors due to gross features of the atmosphere) and the other of which appears at one station only (e.g., errors due to receiver noise). If the common errors are denoted by $\Delta\dot{R}_n$ $(n = 0, 1, 2)$ and the independent errors by $\delta\dot{R}_n$, then the errors in $\dot{p}$ and $\dot{q}$ are

$$\delta\dot{p} = (\Delta\dot{R}_0 + \delta\dot{R}_0) - (\Delta\dot{R}_1 + \delta\dot{R}_1) = \delta\dot{R}_0 - \delta\dot{R}_1$$

$$\delta\dot{q} = \delta\dot{R}_0 - \delta\dot{R}_2$$

It is reasonable to assume that

$$\langle\delta\dot{R}_0^2\rangle = \langle\delta\dot{R}_1^2\rangle = \langle\delta\dot{R}_2^2\rangle = \sigma^2(\dot{R})$$

where $\langle\ \rangle$ indicates the ensemble average. Note that

$$\sigma(\dot{p}) = \sigma(\dot{q}) = (2)^{1/2}\sigma(\dot{R})$$

and that the cross-correlation coefficient of $\dot{p}$ and $\dot{q}$ is

$$\frac{\langle\delta\dot{p}\ \delta\dot{q}\rangle}{\sigma(\dot{p})\ \sigma(\dot{q})} = \frac{\sigma^2(\dot{R})}{2\sigma^2(\dot{R})} = 0.5$$

Errors that occurred in $\dot{R}_0$ and either $\dot{R}_1$ or $\dot{R}_2$, but not in both $\dot{R}_1$ and $\dot{R}_2$, would cause this number to be smaller; and errors that occurred in both $\dot{R}_1$ and $\dot{R}_2$ but not in $\dot{R}_0$ would cause the number to be larger.

In unpublished data provided by personnel of the General Electric Company Radio Guidance Organization, Syracuse, a number of cross-correlation coefficients are given for the noise on $\dot{p}$ and $\dot{q}$ from the GE Mod III guidance system at ETR. They were determined for data from Ranger/Mariner and Mercury flights. The average values of the coefficient at various elevation angles are shown in Table 1. The data indicate that 1) to a considerable extent, the system operates as if the errors in $\dot{p}$ and $\dot{q}$ were generated by three independent noise sources; and 2) there is a tendency for the noise sources to become correlated at low elevation angles.

Table 1 Lateral rate noise cross-correlation coefficients for the GE Mod III guidance system at AMR

Elevation angle, deg	Cross-correlation coefficient of $\dot{p}$ and $\dot{q}$
15°	0.51
10°	0.57
7.5°	0.65
5°	0.54[a]

[a] One sample only.

Sensitivity of $\dot{E}$ and $\dot{A}$

Referring to Fig. 2,

$$\dot{R}_0 = \mathbf{V}\cdot\mathbf{R}_0/R_0$$

$$\dot{R}_1 = \mathbf{V}\cdot R_1/R_1$$

where boldface symbols now indicate vector quantities. If $R_0 \simeq R_1$, then

$$\dot{R}_0 - \dot{R}_1 = \frac{\mathbf{V}\cdot(\mathbf{R}_0 - R_1)}{R_0} = \frac{\mathbf{V}\cdot\mathbf{d}_1}{R_0}$$

and, similarly,

$$\dot{R}_0 - \dot{R}_2 = \mathbf{V}\cdot\mathbf{d}_2/R_0$$

So

$$\dot{R}_0 - \dot{R}_1 = (d\dot{R}_0/\dot{R}_0)\cos E\sin A - d\dot{E}\sin E\sin A + d\dot{A}\cos E\cos A$$

$$\dot{R}_0[1 - (d/\dot{R}_0)\cos E\sin A] - \dot{R}_1 = d\dot{E}\sin E\sin A + d\dot{A}\cos E\cos A$$

and, if $d \ll R_0$,

$$\dot{R}_0 - \dot{R}_1 = -d\dot{E}\sin E\sin\dot{A} + d\dot{A}\cos E\cos A = \dot{p}$$

and, similarly,

$$\dot{R}_0 - \dot{R}_2 = d\dot{E}\sin E\cos A - d\dot{A}\cos E\sin A = \dot{q}$$

From which

$$\dot{E} = \frac{(\dot{R}_0 - \dot{R}_0)\sin A + (\dot{R}_0 - \dot{R}_2)\cos A}{d\sin E}$$

$$\dot{A} = \frac{(\dot{R}_0 - \dot{R}_0)\cos A - (\dot{R}_0 - \dot{R}_4)\sin A}{d\cos E}$$

Then, expressing the errors in $\dot{E}$ and $\dot{A}$ due to the errors in the $\dot{R}_n$ and considering the errors in the $\dot{R}_n$ to be independent random variables of equal variance,

$$\sigma(\dot{E}) = \frac{\sigma(\dot{R})[2(1 + \sin A\cos A)]^{1/2}}{d\sin E}$$

$$\sigma(\dot{A}) = \frac{\sigma(\dot{R})[2(1 - \sin A\cos A)]^{1/2}}{d\cos E}$$

The quantity inside the bracket is plotted in Fig. 1. From this expression it is concluded that, if the errors in $\dot{p}$ and $\dot{q}$ are generated by three independent noise sources, 1) the relative accuracy of the system varies with azimuth, the amount of the variation being from 1 to $3^{1/2}$, and 2) the maxi-

mum accuracy for azimuth lies along the plane that bisects the angle formed by the baselines; the maximum accuracy for elevation lies along the plane perpendicular to this bisector. Physically, the plane for maximum elevation accuracy occurs when

$$\partial\dot{E}/\partial\dot{p} = -(\partial\dot{E}/\partial\dot{q})$$

so that an error that occurs in $\dot{R}_0$ is cancelled when it appears in both $\dot{p}$ and $\dot{q}$. The same statement is true for azimuth also, of course.

Libration Damping and Lunar Mass

IRVING MICHELSON*
Illinois Institute of Technology, Chicago, Ill.

GRAVITATIONALLY oriented satellites are of interest currently because of the possibility they afford to control orientation in space for long time durations without a continuing power requirement. A major design problem is the provision of adequate damping for rotational oscillations; the theory of physical librations of the moon is a useful guide to the underlying dynamics. Consideration of the interactions between librational and orbital motions leads to a new relationship between masses and orbital distances and reveals a condition on friction terms.

Energy dissipation within the moon is directly related to the couple-producing term in the gravitational potential, the sun's effect predominating over the earth's. If the energy of moon's orbital motion around earth is expressed as

$$k^2M_eM_m/-2r$$

and its variation determined by dissipation, the relationship can be written as

$$\frac{M_eM_m}{r^2}\,\delta r + \frac{M_sM_m}{R^3}\delta\phi_1 = 0 \qquad (1)$$

where the Gaussian constant k^2 has been suppressed as a common factor. Earth, moon, and sun masses are denoted M_e, M_m, M_s; earth-moon and sun-moon mean distances are represented by r and R; effects of lunar orientation toward sun and lunar mass asymmetries determine ϕ_1, the explicit form of which is given by MacCullagh's formula (see, e.g., Ref. 1).

Tidal dissipation within the earth due to the proximity of the lunar mass can likewise be related to variation of earth's orbit around sun, giving

$$\frac{M_sM_e}{R^2}\,\delta R + \frac{M_eM_m}{r^3}\,\delta\varphi_2 = 0 \qquad (2)$$

where ϕ_2 likewise depends on the differences between earth's principal inertia moments and the earth-moon orientation.

Although the two Eqs. (1) and (2) do not form a simultaneous system, it is observed that the products of diagonal coefficients form an equality

$$(M_eM_m/M_sM_s) = (r/R)^5 \qquad (3)$$

as is easily verified by direct substitution of known numerical values for each of the quantities contained in this equation. It should be noted that Eq. (3) has not been deduced from (1) and (2), so that a further relationship is implied between the differential coefficients which they contain:

$$\frac{\delta\phi_1}{\delta\phi_2} = \frac{\delta R}{\delta r} \qquad (4)$$

The ratio on the right side of (4) can be evaluated on the basis of orbital considerations (e.g., by requiring the total moment of momentum of earth and moon orbital motions to remain constant). Then the terms on the left relate dissipation within the satellite (moon) to that within the primary. Reciprocity relationships are suggested by the form of (4).

Equation (3) recalls the formula given by Laplace for the radius of the "activity sphere" outside of which the sun's attraction is more important than the earth's on the motion of a third body. If the geometric mean of earth and moon masses is replaced by earth mass, in fact, Eq. (3) becomes identical to Laplace's formula (see, e.g., Ref. 2). That relationship is known to be devoid of precise significance, despite its utility; in contrast, Eq. (3) may be considered surprising in its precision, despite the largely heuristic development given here.

The striking simplicity of the relationship (3), moreover, leads one to expect that it could be found in treatises on celestial mechanics; this is not the case. Nor does the classic literature appear to provide a sound dynamical basis for the equation.

References

[1] Routh, E. J., *Advanced Dynamics of Rigid Bodies* (Dover Publications, Inc., New York, 1955), p. 340.
[2] Tisserand, F., *Mécanique Céleste* (Gauthier-Villars, Paris, 1896), Tome IV, p. 200.

Received August 6, 1964; revision received August 28, 1964.
* Professor of Aerospace Engineering. Member AIAA.

Shock Standoff Distance for Equilibrium Flow Around Hemispheres Obtained from Numerical Calculations

MAMORU INOUYE*
NASA Ames Research Center, Moffett Field, Calif.

KNOWLEDGE of the shock standoff distance yields valuable information concerning the flow field around blunt bodies including first-order estimates of shock-layer radiation and nonequilibrium flow effects. For a given set of freestream conditions and body shape, the standoff distance can be obtained from a numerical solution of the governing differential equations as is described, for example, in Refs. 1 and 2. However, in view of the wide variation in both the possible composition of planetary atmospheres and the possible vehicle trajectories, simple correlations would be useful for design purposes. It is shown in the present note that previously obtained correlations are applicable for a wide range of freestream conditions and gas mixtures.

The inverse method (wherein a shock shape is assumed and a body shape is calculated) has been used to obtain flow-field solutions for air, nitrogen, carbon dioxide, argon, and a mixture of 50% argon, 40% nitrogen, and 10% carbon dioxide. Details of the calculation method can be found in Ref. 1. The equilibrium thermodynamic properties of the gases considered were calculated by Harry Bailey of Ames Research Center. Solutions for hemispheres have been obtained for freestream densities of 10^{-1}, 10^{-3}, and 10^{-5} times earth sea-level density and for velocities in 10,000 fps increments up to approximately 60,000 fps, the upper limit being governed by the maximum temperature of 45,000°R.

The shock standoff distance obtained by the present numerical method is shown in Fig. 1 as a function of the

Received August 6, 1964.
* Research Scientist, Thermo- and Gas-Dynamics Division. Member AIAA.